FACTA UNIVERSITATIS
Series: **Mechanical Engineering**
https://doi.org/10.22190/FUME123456001A

Original scientific paper[*]

EFFECTS OF ROTATION ON UNSTEADY FLUID FLOW AND FORCED CONVECTION IN A ROTATING CURVED SQUARE DUCT WITH SMALL CURVATURE

Mohammad Sanjeed Hasan[1*], Ratan Kumar Chanda[2], Rabindra Nath Mondal[2], Giulio Lorenzini[3]

[1]Department of Mathematics, Bangabandhu Sheikh Mujibur Rahman Science and Technology University, Gopalganj, Bangladesh
[2]Department of Mathematics, Jagannath University, Dhaka, Bangladesh
[3]Department of Engineering and Architecture, University of Parma, Parma, Italy

Abstract. *In recent years, the analysis of flow characteristics through a curved duct has attracted extensive attention to the researchers because it is broadly used in engineering devices. In the ongoing paper, unsteady flow characteristics with energy distribution through a rotating curved square duct with curvature ratio 0.015 has been presented with the aid of spectral method. The key purpose of this study is to explore rotational effects as well as heat transfer in the duct. For this purpose, time-evolution calculation is performed over a wide range of the rotational parameter, the Taylor number* $(-1500 \le Tr \le 1500)$*, where the other parameters such as the Dean number* (Dn)*, the Grashof number* (Gr) *and the curvature* (δ) *are fixed. Firstly, time-dependent behavior is accomplished for both positive and negative rotation, and it is found that the flow instabilities are certainly governed by the change of* Tr *that has been justified by sketching phase spaces. To observe the flow features, two types of flow velocities such as axial and secondary flow and temperature profiles are disclosed for both rotations, and it is elucidated that 2- to 6-vortex solutions are generated for physically realizable solutions. Axial flows show that two high-velocity regions are created which induces secondary flow, and consequently a strong connection between the axial and secondary velocity has been built up. It is observed that as the rotation is increased, the fluid is mixed considerably which boosts heat transfer in the fluid at a great deal. Finally, numerical results have been compared with the available experimental outcomes and a good matching is observed.*

[*]**Received: (this line will be written by the journal; the lines below by the author(s)).**
Corresponding author: Mohammad Sanjeed Hasan
Department of Mathematics, Bangabandhu Sheikh Mujibur Rahman Science and Technology University, Gopalganj-8100, Bangladesh
E-mail: sanjeedlhasan@gmail.com

Key words: *Rotating curved duct, Taylor number, heat-flux, phase space, chaos*

1. INTRODUCTION

Fluid flow and heat transfer through a curved duct continues to be an area of paramount interest in various mechanical and bio-mechanical configurations. Engineers, scientists, and technocrats have over time utilized the ubiquitous nature of ducts to develop machinery, equipment, and industrial processes that have seen the transformation of the world through stages from the first to the fourth industrial revolution. It cannot be an exaggeration to postulate that modernity has to a larger extent depended on the exploitation and manipulation of fluid flow systems through ducts. Numerous investigations on different types of ducts have been studied by many authors. Among them, Mondal et al. [1, 2] and Yanase et al. [3] (square and rectangular duct), Rumsey et al. [4] (U-duct), Chandratilleke et al. [5] (rectangular and elliptical duct), Ahmadloo et al. [6] (helical pipe) can be mentioned for outstanding analysis.

One of the noticeable functions in curved ducts is to examine steady and unsteady flow characteristics. Seven symmetric and four asymmetric solution branches for tightly coiled duct were gained by Liu and Wang [7]. They disclosed the structural change of bifurcation for changing the grid points. Besides, they calculated the dynamical responses for several pseudo-Dean numbers. Yanase et al. [8] used two-dimensional geometry to study transitional behavior for the curved duct flow with a wide range of aspect ratios. Later, Yanase et al. [9] conducted three-dimensional geometry to explore the unsteady behavior for non-rotating curved square duct. They further compared their results with the two-dimensional (2D) outcomes. Time-dependent solutions with respect to the drag and lift coefficient for several Reynolds numbers and gap spacing parameters across multiple staggered rows of cylinders have been represented by Nazeer et al. [10]. They validated their periodic oscillation by power spectrum analysis. Zhou et al. [11] used particle image velocimetry (PIV) method to compare the unsteady flow characteristics in half and fully dimpled circular cylinder for large Reynolds numbers. Zhang et al. [12] conducted unsteady behavior for four square-shaped cylinders where the cylinders were kept at an equal distance from each other. Hashemi et al. [13] measured the fluctuation of the velocity components regarding time through the curved pipe. Unsteady behaviors in a square enclosure with mixed convection have been steered out by Zhang et al. [14]. Wang and Yang [15] numerically and experimentally reported dynamical responses of the flow through the curved duct for various Dean numbers. Transient behavior with thermal analysis in porous cavities for large aspect ratios has been calculated by Arpino et al. [16]. Mondal et al. [17, 18] computed the change of unsteady flow behavior in the cooling and heating sidewalls for several Dean numbers, Grashof number, aspect ratio and Taylor number respectively. They justified their oscillating flows by drawing the phase space of the time-evolution results. Hasan et al. [19, 20] obtained three different types of flow oscillations such as steady-state, periodic, and chaotic flow for both rotating and non-rotating curved duct with small and medium curvatures respectively. Islam et al. [21] adopted function expansion and collocation method to seek out the unsteady solutions for rotating curved rectangular duct flow. Kurtulmus et al. [22] observed the Nusselt number effect in flow transition for converging and diverging channel. Zheng et al. [23] used

$k-\omega$ turbulence model in the serpentine tube to obtain the temperature oscillation and the effects of centrifugal and buoyancy force in the flow transition. Among the cited papers, most of the authors showed only flow transition; some of them investigated power spectrum density to justify the flow oscillation. But they did not illustrate the phase space which is an important phenomenon for regular and irregular flow transition. The present study, therefore, represents unsteady flow characteristics, and the flow transition is meticulously justified by sketching phase space of the time change of flux that gives a clear view for the periodic, multi-periodic and chaotic flow.

Flow visualization is another significant material for the duct because it recounts the effects of fluid and heat transfer mixing. It is known that Dean [24] was the first who derived the governing equations of curved ducts. He related that the two-vortex secondary flow converted into four-vortex at the limit points of the steady solution and these two-vortex are designated as the *Dean vortex* after his name. He also demonstrated that there are three types of potency such as centrifugal force, Coriolis force and body force worked in the fluid flow. Here, it is noted that the centrifugal and Coriolis forces are influenced by the duct curvature and rotation, respectively. Ozaki and Maekawa [25] showed curvature effects in the curved duct flow. Numerical and experimental investigations with heat transfer through curved rectangular and elliptical ducts were illustrated by Chandratilleke et al. [26]. Ferdows et al. [27] explained the effects of Dean number in the helical duct for different rotational numbers. Bayat et al. [28] developed numerical and experimental flow model to demonstrate the upshot of curvature and kinematic viscosity for curved and spiral micro-channel. Li et al. [29] pursued the numerical study of two-dimensional flow behavior for changing the curvature and aspect ratio of the duct. They further performed flow velocity with three-dimensional (3D) contours of the secondary flow where the flow fields were measured by using the particle image velocimetry technique. Watanabe and Yanase [30] attempted to develop a three-dimensional model to visualize the flow structures. Nowruzi et al. [31] used the energy gradient method to report flow structure through a curved rectangular duct with 120° inlet. Considering the perturbation method as the main tool, Norouzi and Biglari [32] accomplished the formation of secondary flow structures. They further sketched the vector plot of the secondary flow. Razavi et al. [33] have performed flow structure, heat and entropy transmission through a rotating curved channel where they applied the second law of thermodynamics. The influence of centrifugal and hydrodynamic instability in unsteady behavior and heat transfer was attained by Hasan et al. [34, 35]. Sasmito et al. [36] evaluated the enhancement of heat transfer for the nano-fluid particle in coiled ducts. Al-Juhaishi et al. [37] elucidated the friction losses and heat transfer in a curved channel. They demonstrated that heat transfer is dramatically induced by the baffles of the channel. Zhang et al. [38] proposed a 3D scheme to demonstrate the influence of centrifugal force in the heat transfer through the curve channel. Zhang et al. [39] illustrated the chaotic flow and heat transfer under a critical buoyancy and rotation number. Schindler et al. [40] calculated the total amount of heat transfer and the fluid mixing when the turbulent flows occurred in a heated duct with square cross-section. However, it is pronounced that there is a strong relationship between the axial and secondary flow velocity and the isotherms, which has not been explored in literature till today. The ongoing paper, therefore, represents a strong connection between the flow velocity and the isotherms together with

flow transition and convective heat transfer in the duct. Finally, a comparison between the numerical and experimental outcomes has been presented to validate the current study.

2. FLOW MODEL AND GOVERNING EQUATIONS

A two-dimensional (2D) fully developed laminar flow through a curved square duct with constant curvature is considered as illustrated in Figure 1. The relevant notations with coordinate system are shown in Figure 1. It is noted that the lower wall of the duct is heated while the upper wall cooled, the others walls being thermally insulated. The continuity equation, Navier-Stokes equations and energy equation in cylindrical coordinate system are written as,

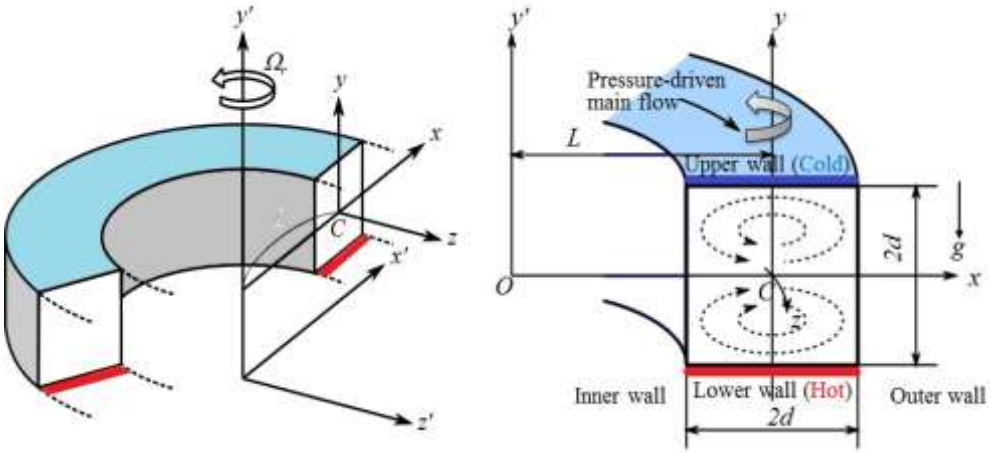

(a) (b)

Fig. 1 (a) The physical model, (b) Cross-sectional view of curved duct.

Continuity equation:

$$\frac{\partial v_r}{\partial r}+\frac{1}{r}\frac{\partial v_\theta}{\partial \theta}+\frac{\partial v_y}{\partial y}+\frac{v_r}{r}=0 \tag{1}$$

Navier-Stokes equations:

$$\frac{\partial v_r}{\partial t}+(v.\nabla)v_r-\frac{v_\theta^2}{r}=-\frac{1}{\rho}\frac{\partial P}{\partial r}+\nu\left(\tilde{\Delta}v_r-\frac{v_r}{r^2}-\frac{2}{r^2}\frac{\partial v_\theta}{\partial \theta}\right) \tag{2}$$

$$\frac{\partial v_\theta}{\partial t}+(v.\nabla)v_\theta+\frac{v_r v_\theta}{r}=-\frac{1}{\rho r}\frac{\partial P}{\partial \theta}+\nu\left(\tilde{\Delta}v_\theta-\frac{v_\theta}{r^2}+\frac{2}{r^2}\frac{\partial v_r}{\partial \theta}\right) \tag{3}$$

$$\frac{\partial v_y}{\partial t}+(v.\nabla)v_y=-\frac{1}{\rho}\frac{\partial P}{\partial y}+\nu\tilde{\Delta}v_r+\beta gT \tag{4}$$

Energy equation:

$$\frac{\partial T}{\partial t}+(v.\nabla)T=\kappa\tilde{\Delta}T \tag{5}$$

Here, $v.\nabla=v_r\frac{\partial}{\partial r}+\frac{v_\theta}{r}\frac{\partial}{\partial\theta}+v_y\frac{\partial}{\partial y}$, $\tilde{\Delta}=\frac{\partial^2}{\partial r^2}+\frac{1}{r}\frac{\partial}{\partial r}+\frac{1}{r^2}\frac{\partial^2}{\partial\theta^2}+\frac{\partial^2}{\partial y^2}$,

Here, v_x, v_y and v_θ are velocity components in r, θ and y axis respectively. Now, the Equations (1) to (5) are non-dimensionalized by the assumptions:

$$r=L+dx',\ y=hy',\ L\theta=-dz',\ T=T'\Delta T,\ v_r=v_x=U_0u',\ v_y=v_y=U_0v',$$

$$v_\theta=-v_z=U_0w',\ \rho=\rho_0U_0^2P',\ G=-\frac{\partial P}{\partial z'},\ \in=\sqrt{\frac{2d}{L}}=\sqrt{2\delta},\ \delta=\frac{d}{L}$$

In this study, δ is the curvature of the duct identified as the ratio of the width and the radius of curvature. The study is based on two-dimensional flow which is uniform in the $z'-$direction and so $\frac{\partial p'}{\partial z'}=0$. After non-dimensionalization, the transformed Equations (1) to (5) can be written as,

Continuity equation:

$$\frac{\partial u'}{\partial x'}+\frac{\partial v'}{\partial y'}+\frac{\delta u'}{1+\delta x'}+\frac{1}{1+\delta x'}\frac{\partial w'}{\partial z'}=0 \tag{6}$$

Navier-Stokes equations:

$$\frac{\partial u'}{\partial t'}+(v'.\nabla')u'-\frac{1}{2}\in^2\frac{w'^2}{1+\delta x'}=-\frac{\partial P'}{\partial x'}+\frac{\in}{Dn}\left(\tilde{\Delta}_2'u'-\frac{\delta^2u'}{(1+\delta x')^2}\right) \tag{7}$$

$$\frac{\partial v'}{\partial t'}+(v'.\nabla')v'=-\frac{\partial P'}{\partial y'}+\frac{\in}{Dn}\tilde{\Delta}_2'v'+\frac{\beta g\Delta Tl}{U_0^2}T' \tag{8}$$

$$\frac{\partial w'}{\partial t'}+(v'.\nabla')w'+\frac{1}{2}\in^2\frac{u'w'}{1+\delta x'}=-\frac{G}{1+\delta x'}+\frac{\in}{Dn}\left(\tilde{\Delta}_2'w'-\frac{\delta^2u'}{(1+\delta x')^2}\right) \tag{9}$$

Energy equation:

$$\frac{\partial T'}{\partial t'}+(v'.\nabla')T'=\frac{\kappa}{dU_0}\tilde{\Delta}_2'T' \tag{10}$$

Where, $(v'.\nabla')=u'\frac{\partial}{\partial x'}+v'\frac{\partial}{\partial y'}$ and $\tilde{\Delta}_2'=\frac{\partial^2}{\partial x'^2}+\frac{\partial}{\partial y'^2}+\frac{\delta}{1+\delta x'}\frac{\partial}{\partial x'}$

Now, introducing the vorticity vector and the stream function along the x'- and y'-directions respectively, we have

$$\Omega'=\frac{\partial v'}{\partial x'}-\frac{\partial u'}{\partial y'}=-\frac{1}{1+\delta x'}\left(\frac{\partial^2}{\partial x'^2}+\frac{\partial^2}{\partial y'^2}-\frac{\delta}{1+\delta x'}\frac{\partial}{\partial x'}\right) \tag{11}$$

$$u'=\frac{1}{1+\delta x'}\frac{\partial\psi'}{\partial y'} \quad \text{and} \quad v'=-\frac{1}{1+\delta x'}\frac{\partial\psi'}{\partial x'} \tag{12}$$

Differentiating (8) and (9) with respect to x' and y' and subtracting we have,

$$\frac{\partial \Omega'}{\partial t'}+\left(u'\frac{\partial}{\partial x'}+v'\frac{\partial}{\partial y'}\right)\Omega'-\frac{\delta u'}{1+\delta x'}\Omega'+\frac{\in^2 w'}{1+\delta x'}\frac{\partial w'}{\partial y'}$$
$$=\frac{\in}{Dn}\left(\tilde{\Delta}_2'-\frac{\delta^2}{1+\delta x'}\right)\Omega'+\frac{\beta g\Delta Tl}{U_0^2}\frac{\partial T'}{\partial x'} \tag{13}$$

The simplified equations are found after removing the prime signs from the primitive equations and finally we obtain,

$$(1+\delta x)\frac{\partial w}{\partial t}+\frac{\partial(w,\psi)}{\partial(x,y)}-Dn+\frac{\delta^2 w}{1+\delta x}=(1+\delta x)\Delta_2 w-\frac{\delta w}{(1+\delta x)}\frac{\partial \psi}{\partial y}+\delta\frac{\partial w}{\partial x}-\delta Tr\frac{\partial \psi}{\partial y}, \tag{14}$$

$$\left(\Delta_2-\frac{\delta}{1+\delta x}\frac{\partial}{\partial x}\right)\frac{\partial \psi}{\partial T}=-\frac{1}{(1+\delta x)}\frac{\partial(\Delta_2\psi,\psi)}{\partial(x,y)}+\frac{\delta}{(1+\delta x)^2}\left[3\delta\frac{\partial^2\psi}{\partial x^2}-\frac{3\delta^2}{1+\delta x}\frac{\partial \psi}{\partial x}\right]$$
$$-\frac{2\delta}{1+\delta x}\frac{\partial}{\partial x}\Delta_2\psi+\frac{\delta}{(1+\delta x)^2}\left[\frac{\partial \psi}{\partial y}\left(2\Delta_2\psi-\frac{3\delta}{1+\delta x}\frac{\partial \psi}{\partial x}+\frac{\partial^2\psi}{\partial x^2}\right)-\frac{\partial \psi}{\partial x}\frac{\partial^2\psi}{\partial x\partial y}\right]+w\frac{\partial w}{\partial y} \tag{15}$$
$$+\Delta_2^2\psi-Gr(1+\delta x)\frac{\partial T}{\partial x}+\frac{1}{2}Tr\frac{\partial w}{\partial y},$$

$$\frac{\partial T}{\partial t}+\frac{1}{(1+\delta x)}\frac{\partial(T,\psi)}{\partial(x,y)}=\frac{1}{Pr}\left(\Delta_2 T+\frac{\delta}{1+\delta x}\frac{\partial T}{\partial x}\right). \tag{16}$$

Where, $\Delta_2=\frac{\partial^2}{\partial x^2}+\frac{\partial^2}{\partial y^2}$ and $\frac{\partial(f,g)}{\partial(x,y)}=\frac{\partial f}{\partial x}\frac{\partial g}{\partial y}-\frac{\partial f}{\partial y}\frac{\partial g}{\partial x}$

It is noted that Equations (14) – (16) are invariant with respect to the horizontal axis; Dn, Gr, Tr and Pr are the non-dimensional parameters and addressed as the Dean number, the Grashof number, the Taylor number and the Prandtl number, respectively defined as,

$$Dn=\frac{Gd^3}{\mu\upsilon}\sqrt{\frac{2d}{L}},\ Gr=\frac{\beta g\Delta T\, d^3}{\upsilon^2},\ Tr=\frac{2\sqrt{2\delta}\Omega_T d^3}{\upsilon\delta},\ Pr=\frac{\upsilon}{\kappa}$$

The bounder conditions of the axial velocity (w) and the sectional stream velocity (ψ) are,

$$w(\pm1,y)=w(x,\pm1)=\psi(\pm1,y)=\psi(x,\pm1)=\frac{\partial \psi}{\partial x}(\pm1,y)=\frac{\partial \psi}{\partial y}(x,\pm1)=0 \tag{17}$$

and the boundary conditions for isotherm (T) are taken as,

$$T(x,1)=1,\ T(x,-1)=-1, T(\pm1,y)=y \tag{18}$$

In the current study, water is the working fluid $(Pr=7.0)$ and throughout this study we performed numerical simulation for Dn=1000, Gr=100, $\delta=0.015$ and the Taylor

number (Tr) varies from -1500 to 1500. Details of the governing equations are represented in Mondal et al. [2].

3. NUMERICAL CALCULATIONS

3.1 Method of Numerical Design

In the existent study, the spectral method is used to obtain the numerical solution of the flow and heat transfer in a curve duct of square cross section. Expansion of the polynomial functions is one of the main objects of this method. That is, the variables are expanded in the series of functions consisting of the Chebyshev polynomials. The expansion functions $\varphi_n(x)$ and $\psi_n(x)$ are disclosed as,

$$\left.\begin{aligned}\varphi_n(x) &= (1-x^2)\ \ C_n(x),\\ \psi_n(x) &= (1-x^2)^2\ \ C_n(x)\end{aligned}\right\} \tag{19}$$

where $C_n(x)$ is the n^{th} order Chebyshev polynomials defined by $C_n(x) = \cos\left(n\cos^{-1}(x)\right)$. Furthermore, $w(x, y, t)$, $\psi(x, y, t)$ and $T(x, y, t)$ are expanded in terms of $\varphi_n(x)$ and $\psi_n(x)$ as:

$$\left.\begin{aligned}w(x,y,t) &= \sum_{m=0}^{M}\sum_{n=0}^{N} w_{mn}(t)\varphi_m(x)\varphi_n(y)\\ \psi(x,y,t) &= \sum_{m=0}^{M}\sum_{n=0}^{N} \psi_{mn}(t)\psi_m(x)\psi_n(y)\\ T(x,y,t) &= \sum_{m=0}^{M}\sum_{n=0}^{N} T_{mn}(t)\varphi_m(x)\varphi_n(y) - y\end{aligned}\right\} \tag{20}$$

where M and N are the truncation numbers in the x- and y-directions respectively, and w_{mn}, ψ_{mn} and T_{mn} are the coefficients of expansion which are substituted into the basic Eqs. (14) - (16) and the collocation method is applied. As a result, the nonlinear algebraic equations for w_{mn}, ψ_{mn} and T_{mn} are obtained. The collocation points are taken to be

$$x_i = \cos\left[\pi\left(1-\frac{i}{M+2}\right)\right], \qquad y_i = \cos\left[\pi\left(1-\frac{i}{N+2}\right)\right] \tag{21}$$

where i = 1,….., M+1 and j = 1,….., N+1. In order to calculate the unsteady solutions, the Crank-Nicolson and Adams-Bashforth methods together with the function expansion (20) and the collocation methods are applied to equations (14) - (16). Details of this method are available in Gottlieb and Orszag [41] and Mondal [42].

3.2 Flux through the Duct

In the impending work, the flux (total flow) through the duct is elucidated as,

$$Q' = \int_{-d}^{d}\int_{-d}^{d} w'dx'dy' = VdQ \tag{22}$$

where, Q' is the dimensional heat-flux and $\overline{w}'$ is the mean axial velocity enumerated by

$$\overline{w}' = \frac{Q\nu}{4d} \tag{23}$$

However, after making dimensionless of equation (22), the flux Q is written as

$$Q = \int_{-1}^{1}\int_{-1}^{1} wdxdy \tag{24}$$

3.3 Grid Efficiency

Here, grid efficiency is conducted for the truncation numbers *M* and *N*. As the paper deals with square duct flow, so *M* and *N* are considered as equal. In this study, the values of axial flow and heat flux for both positive and negative rotation is taken for different truncation number where the parameters of governing equations are fixed. Table 1 shows grid accuracy and it is seen that the values do not show substantial change for increasing or decreasing the truncation numbers. To get sufficient accuracy, *M* = (*N*) = 20 has been taken for numerical simulation.

Table 1 The values of *Q* and *w* (0, 0) for various *M* and *N* at *Dn* = 1000, *Gr* = 100, *Tr* = 500 (positive rotation) & *Tr* = -500 (negative rotation) and $\delta = 0.015$

	M	*N*	*Q*	*w* (0,0)
Positive Rotation	16	16	291.1740208493	382.6415407505
	18	18	291.4440637777	378.9279648439
	20	**20**	**291.5043954187**	**378.2773776991**
	22	22	291.5491957619	379.0478252693
	24	24	291.5511087350	379.0911636619
Negative Rotation	16	16	322.2820420248	381.0710697212
	18	18	322.2817278220	381.0904822522
	20	**20**	**322.2795158289**	**381.3121404054**
	22	22	322.2790330741	381.4151170197
	24	24	322.2787357133	381.5126278631

4. RESULTS

In the following, time-evolution calculation of the unsteady solution is performed for fixed Dean number $(Dn = 1000)$, Grashof number $(Gr = 100)$ and curvature $(\delta = 0.015)$ where the rotational parameter, the Taylor number is varied from -1500 to 1500. The programming algorithm of the governing equations is developed with the Crank-Nicolson method, Adam-Bashforth method and function collocation method simultaneously. Moreover, two types of flow velocity including axial and the secondary flow and the temperature profiles characteristics in positive and negative rotation are also explored in this study.

4.1 Time-dependent Flow Behaviors

4.1.1 Case I: Positive Rotation $(0 \le Tr < 1500)$

Initially, we consider small rotation in the positive direction, for example, $Tr = 10$. At $Tr = 10$, time-dependent of the unsteady flow is analyzed and it is found that the unsteady solution gives multi-periodic result in the *time vs. heat-flux* plane as plotted in Figure 2(a). The multi-periodic behavior is also endorsed by the phase space analysis as depicted in Figure 2(b). Here, the phase space is calculated from the time-dependent solution and sketched in the $\lambda - \gamma$ plane, where γ is prescribed as $\gamma = \int\int \psi dxdy$. The phase space in Figure 2(b) narrates the ability of the tremble as a function of frequency at which the frequencies have potent and at which the frequencies are feeble. Two types of flow velocity, axial and secondary flow and temperature profiles are shown in Figure 3. It is observed from the axial flow that the particle have pushed at the inner wall of the duct. From the secondary flow, 2- to 4-vortex solution is found for $Tr = 10$. It is found that there is a strong bond between the axial and the secondary flow. At $t = 26.00$ & 26.30, two high-velocity regions are produced at the outer wall of the duct, as a result, two new vortices are generated. Here, the newly produced 2-vortex is known as *Dean vortices* and the previous 2-vortex is called *Ekman vortex*. It is further illustrated that the two new vortexes at $t = 26.00$ are smaller than that at $t = 26.30$. This is happened because of the influence of the axial flows. More explicitly, at $t = 26.00$, only two high-velocity regions are created at the outer wall of the duct where no dumbbells are formed. On the other hand, at $t = 26.30$, two high velocity regions are generated with two dumbbells at the outer-upper and outer-lower wall of the duct. As a result, newly creating 2-vortex at $t = 26.30$ are more larger than the 2-vortex formed at $t = 26.00$. It is also remarked that due to dumbbells at $t = 26.30$ the flow velocity is stronger enough than that at $t = 26.00$. This has been created because of the centrifugal force of the duct. Temperature profiles show that heat is transferred exceedingly at $t = 26.00$ & 26.30 within the time $(25.90 \le t \le 26.40)$. It is easily demonstrated that when the flow velocity is strong, the heat is more transferred which proves that the fluid is mixed excessively when the velocity of the flows are strong.

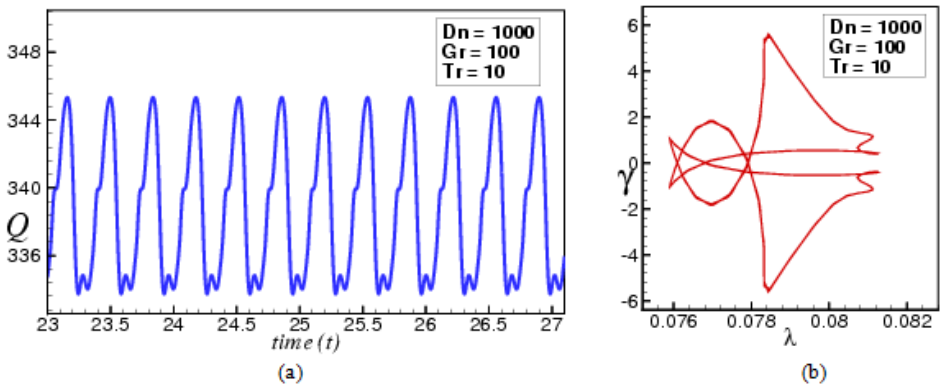

Fig. 2 (a) Time-dependent behavior and (b) Phase space for $Tr = 10$.

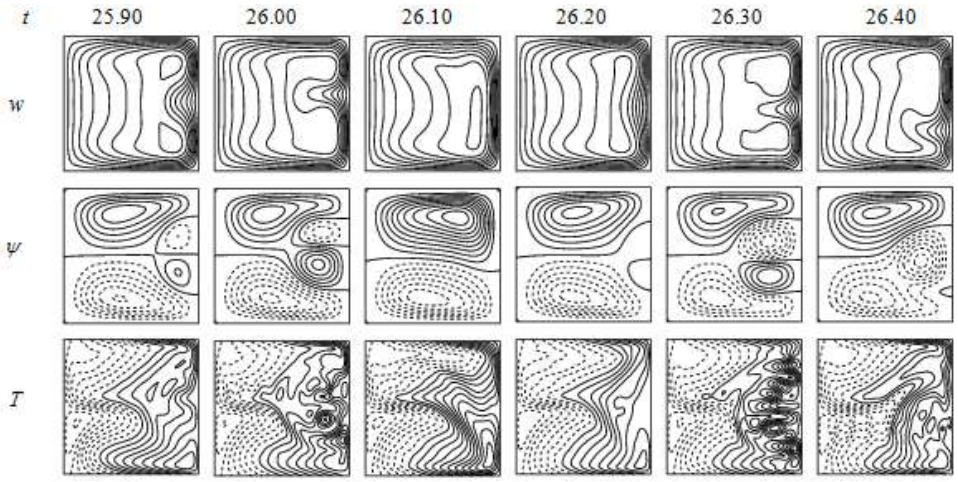

Fig. 3 Contours of axial velocity (topmost), stream function (central) and isotherm (lowermost) for $Tr = 10$.

If the rotational speed is increased, the multi-periodic oscillation converts into steady-state solution. Figure 4(a) shows steady-state solutions for $Tr = 200$ & 400 . It is observed that the value of the heat-flux is decreased for raising *Tr*. Axial flow, secondary flow and isotherm are visualized in Figure 4(b). It is said from the steady-state solutions that only symmetric 2-vortex secondary flow patterns are found.

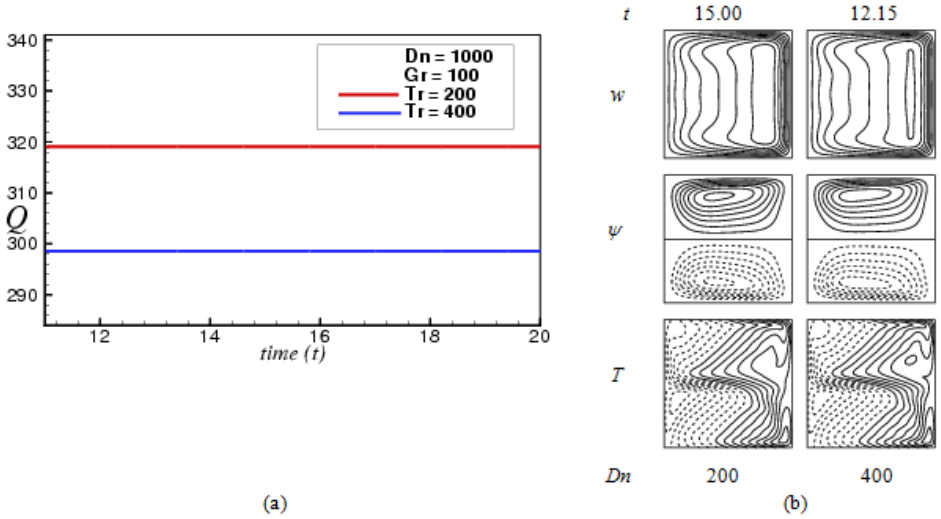

Fig. 4 (a) Time-dependent behavior, (b) Contours of axial velocity (topmost), stream function (central) and isotherm (lowermost) for $Tr = 200$ & 400 .

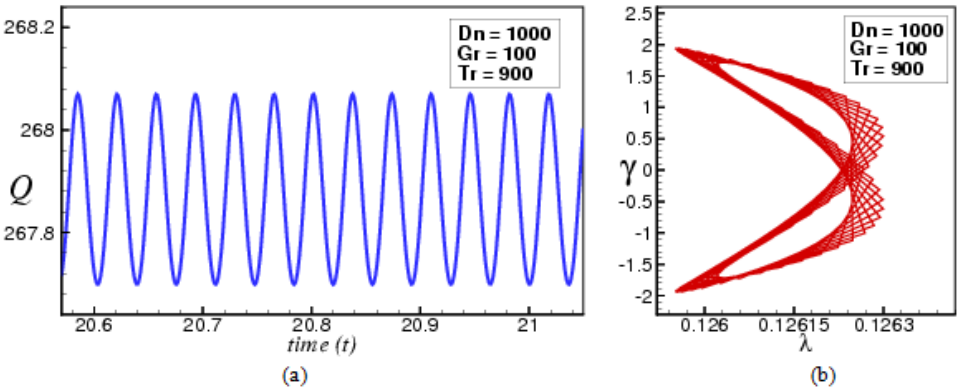

Fig. 5 (a) Time-dependent behavior and (b) Phase space for $Tr = 900$.

When Tr crosses over 750, regular oscillation starts. Here, we investigate time-development of the unsteady solution for $Tr = 900$ and the outcomes are plotted in Figure 5(a). To ensure more about periodic oscillation, phase space is also enumerated as displayed in Figure 5(b). It is explained from phase space that the path line creates multiple orbits in the oscillation. So, it can be demonstrated that the flow is in the initial stage of multi-periodic oscillation rather than periodic that is created at $Tr = 900$. This is occurred because the flow characteristics are significantly affected by the coriolis force. Two types of flow velocity, axial and symmetric and asymmetric 2-vortex secondary flows and isotherm are shown in Figure 6.

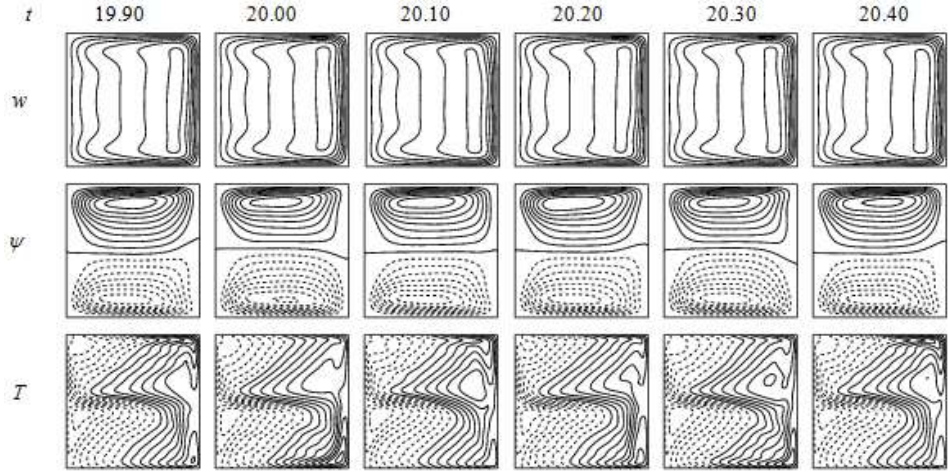

Fig. 6 Contours of axial velocity (topmost), stream function (central) and isotherm (lowermost) for $Tr = 900$.

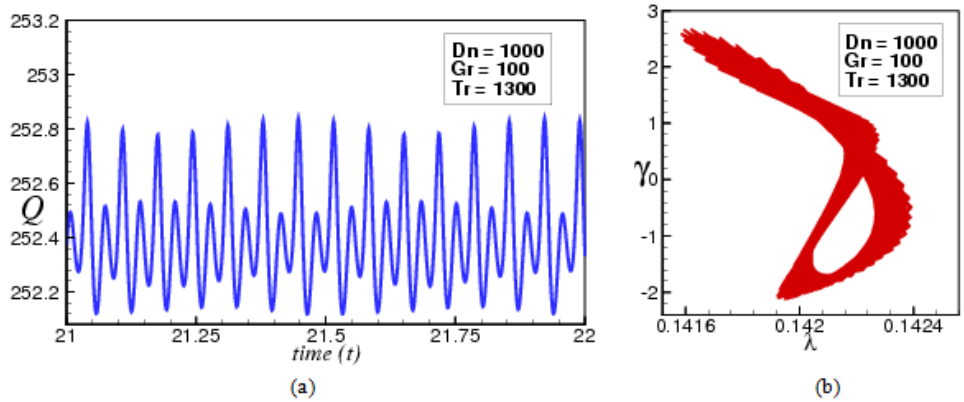

Fig. 7 (a) Time dependent behavior and (b) Phase space for $Tr = 1300$.

Due to disorientation in periodic and multi-periodic flow in before, we investigate time-dependent solution from $Tr = 950$ to $Tr = 1300$. It is elucidated that the oscillation for the required Tr is certainly multi-periodic. Figure 7(a) represents the multi-periodic flow for $Tr = 1300$. The phase space drawn in Figure 7(b) exposes that the multiple orbits are produced and the path lines overlap each other. It is further expressed that the area of steam function is growing for increasing Tr. So it can be said that multi-periodic oscillation is nearly at the terminal stage. Flow patterns with temperature profiles are exhibited in Figure 8. It is noticed that 2-vortex asymmetric secondary flow are created at $Tr = 1300$ where the axial flow and the temperature profiles bear their usual significances.

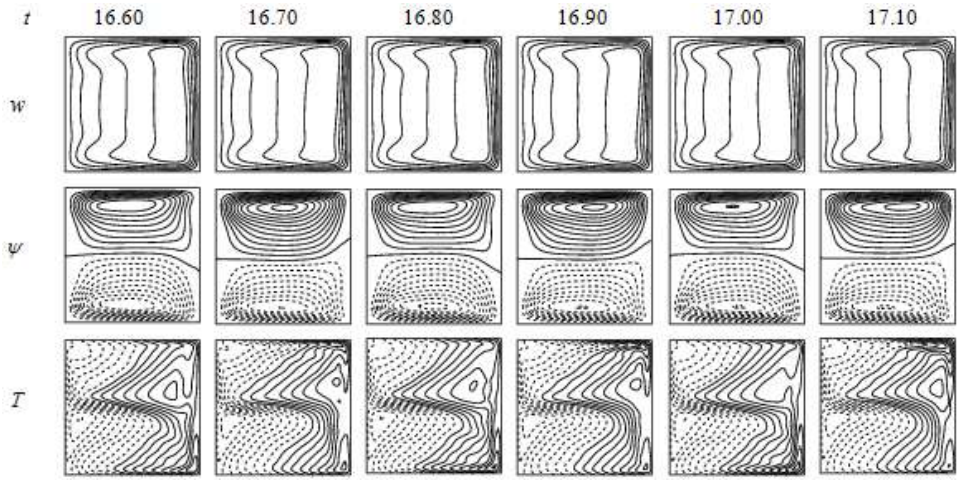

Fig. 8 Contours of axial velocity (topmost), stream function (central) and isotherm (lowermost) for $Tr = 1300$.

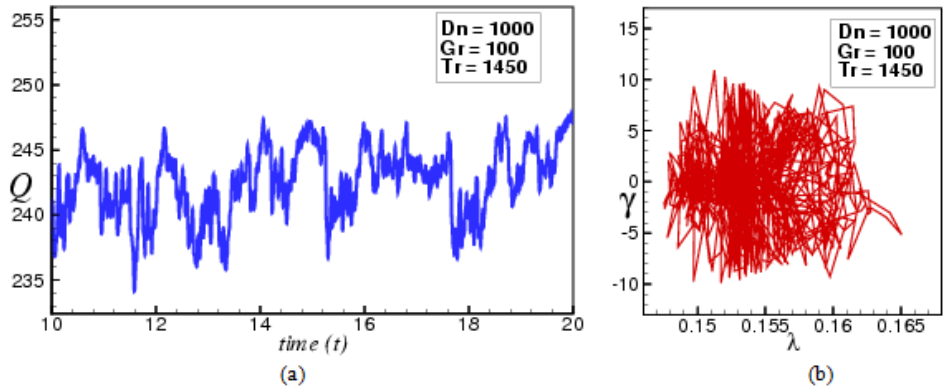

Fig. 9 (a) Time-dependent behavior and (b) Phase space for $Tr = 1450$.

If the *Tr* is raised more, the multi-periodic oscillation shifted into chaotic oscillation. The chaotic oscillation starts at $Tr = 1150$ approximately and continues till $Tr = 1500$. Figure 9(a) discloses the unsteady flow characteristics for $Tr = 1450$. It is seen that the flow oscillates more at the chaotic flow than the periodic/ multi-periodic flows and the density of the oscillation is enhanced for increasing *Tr*. Phase space of the chaotic oscillations is also enumerated as shown in Figure 9(b), which justifies the flow configuration as it is anticipated. From the phase space, the path lines pass over each other in the $\lambda - \gamma$ plane, as a result, a critical flow characterizes has been found. It can be said that due to increase of *Tr*, the flow oscillation is enhanced gradually. As a consequence, the vibration of fluid particle increases, for this reason, the fluids are mixed

which prolongs the overall heat transfer in flow. Axial flow, secondary flow and isotherms are depicted in Figure 10 for $Tr = 1450$.

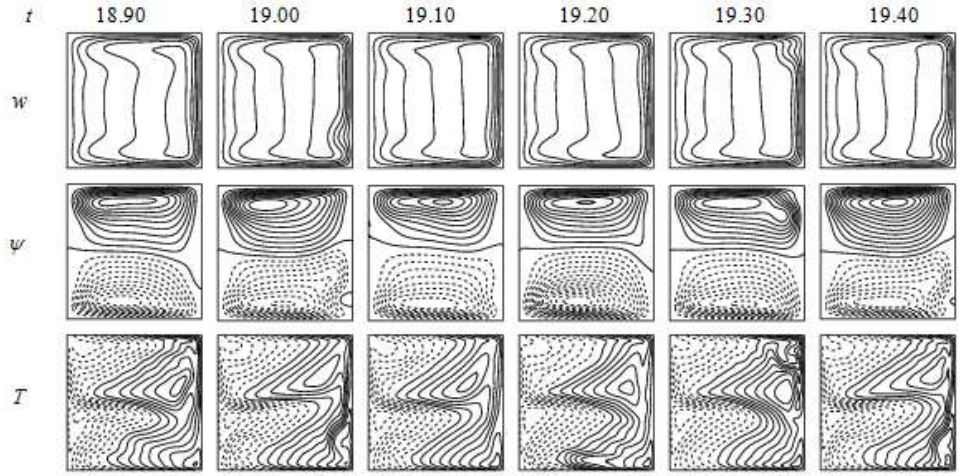

Fig. 10 Contours of axial velocity (topmost), stream function (central) and isotherm (lowermost) for $Tr = 1450$.

4.1.2 Case II: Negative Rotation $(-1500 < Tr < 0)$

Here, at first, we accomplish the time-development of the unsteady flow for $Tr = -30$, and it represents the multi-periodic oscillation as shown in Figure 11(a). Phase space is further plotted in Figure 11(b) for explaining the multi-periodic oscillation properly. It is demonstrated form the phase space that the path lines coincide at the starting point after completing two cycles. Two types of flow velocity such as axial and secondary flows and corresponding temperature profiles are exhibited in Figure 12. Axial flow patterns describe that, when two-vortex asymmetric solutions consist, the flow velocity pushes at the outer wall of the duct $(t = 17.70)$. It is obtained that the axial velocity forms a dumbbell at the outer wall of the duct at $t = 17.60$ and as a consequence, another vortex has been appeared in the lower part of the duct. At time $t = 17.80$, two high-velocity regions are generated, so the secondary flow gives 4-vortex solution. It is also observed that at $t = 17.90$, two high-velocity regions are found where the upper region is smaller than the lower region and single dumbbell is produced at the lower wall; for this reason, four-vortex secondary flow is obtained where the lower vortex is bigger than the upper one and the upper vortex is weaker than the lower one. The isotherms illustrate that when the axial velocity does not produce high-velocity regions, the density of the isotherm stream is less but the opposite criteria are found when axial velocity generates the high-velocity regions. So it can be easily said that secondary vortex as well as isotherms are certainly influenced by the axial flows of the duct.

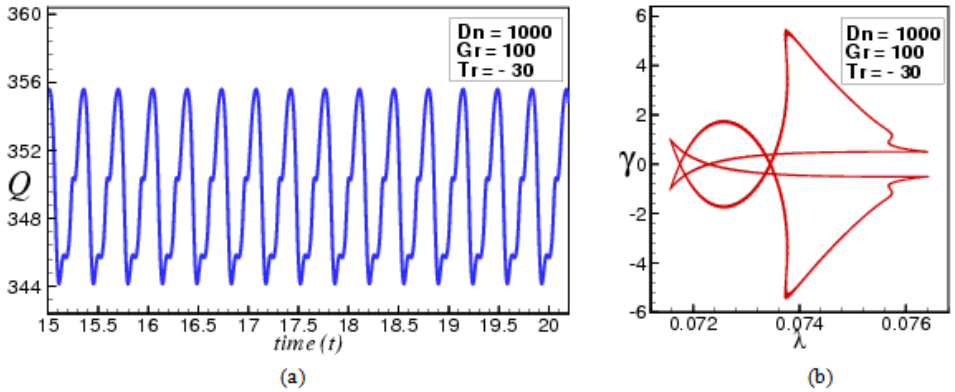

Fig. 11 (a) Time-dependent behavior and (b) Phase space for $Tr = -30$.

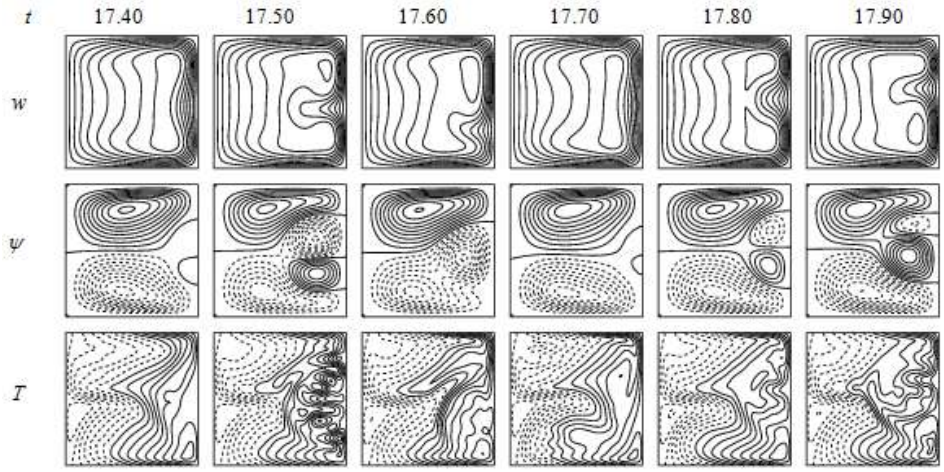

Fig. 12 Contours of axial velocity (topmost), stream function (central) and isotherm (lowermost) for $Tr = -30$.

If Tr is increased in the negative direction, the unsteady solutions are converted into steady-state solution. The steady-state flow initiates at $Tr = -160$ and terminates at $Tr = -390$ which are found from the linear stability analysis. Figure 13(a) displays the steady-state solution at $Tr = -230$. Flow characteristics (axial and secondary) and temperature profiles are visualized in Figure 13(b), where 4-vortex symmetric secondary vortices are noted for the steady-state solution.

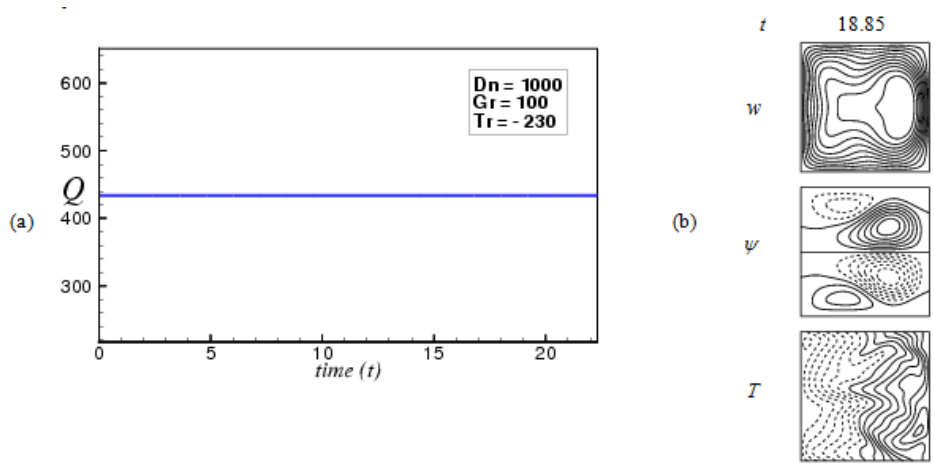

Fig. 13 (a) Time dependent behavior, (b) Contours of axial velocity (topmost), stream function (central), isotherm (lowermost) for $Tr = -230$.

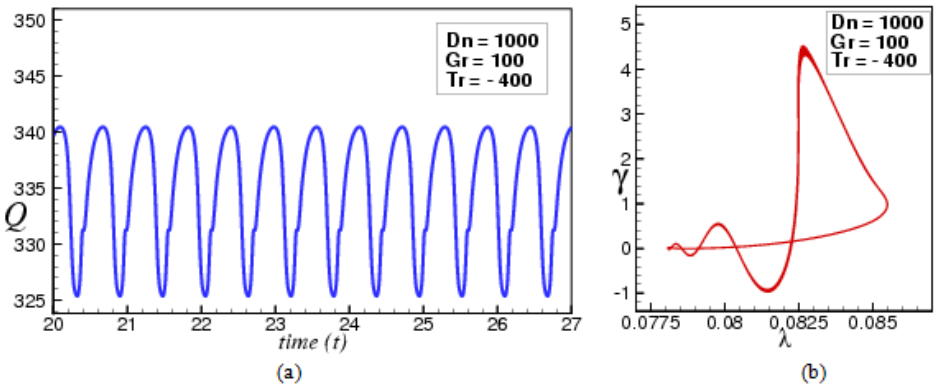

Fig. 14 (a) Time-dependent behavior and (b) Phase space for $Tr = -400$.

If Tr is increased further, the steady-state solution turns into multi-periodic oscillation at $Tr = -400$ as shown in Figure 14(a). The phase space of the multi-periodic oscillation is exposed in Figure 14(b), which demonstrates that the path lines consist of two multiple orbits before meeting at the starting point. Two types of flow velocity, axial and secondary flow and isotherms are revealed in Figure 15. An interesting types of flow properties are found at $Tr = -400$. From the axial flow, the flow velocity has pushed to the inner wall of the duct. The secondary vortices of the flow patterns depict that due to the coriolis force in the negative direction the dotted lines are produced at the upper wall of the duct and the solid lines are created at the lower wall of the duct. As a consequence of these types of rotation of negatively, the Ekman vortices have originated at the inner wall of the duct. Here, a connection between axial flow, secondary flow and isotherms is also obtained. For example, at $t = 14.45$, two high velocity regions with two dumbbells of

axial flow are produced at the inner wall of the duct, as a consequence, four-vortex secondary flow is generated where the two new vortices are generated at the inner wall of the duct. Besides, the lower dumbbells of axial flow are smaller than that at the upper one for this reason although the two vortices look similar, the lower vortex is smaller than the upper vortex. However, in brief, despite of being change direction of the axial velocity, the meaning of flow characteristics are same in axial and secondary flow. Mainly, the flow velocity directions changes because of the rotation of the duct. It is certain that the change of direction of the flow velocity affects the fluid mixing and the overall heat transfer in the flow.

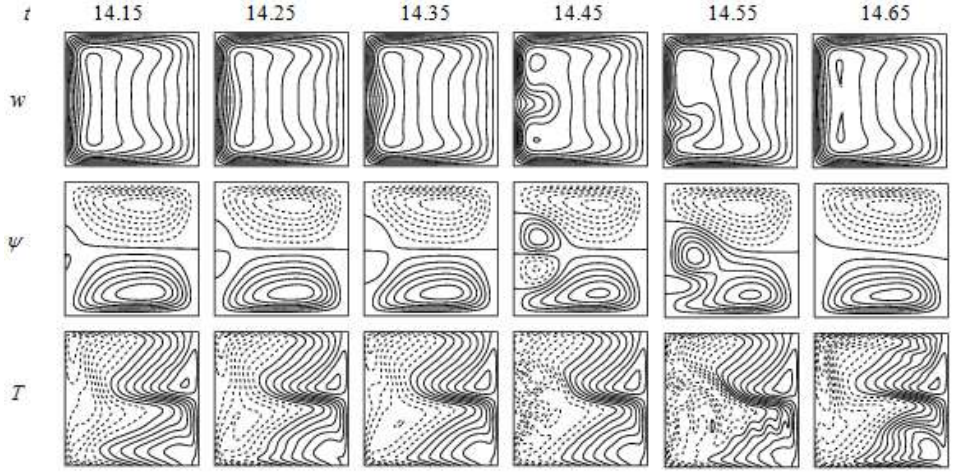

Fig. 15 Contours of axial velocity (topmost), stream function (central) and isotherm (lowermost) for $Tr = -400$.

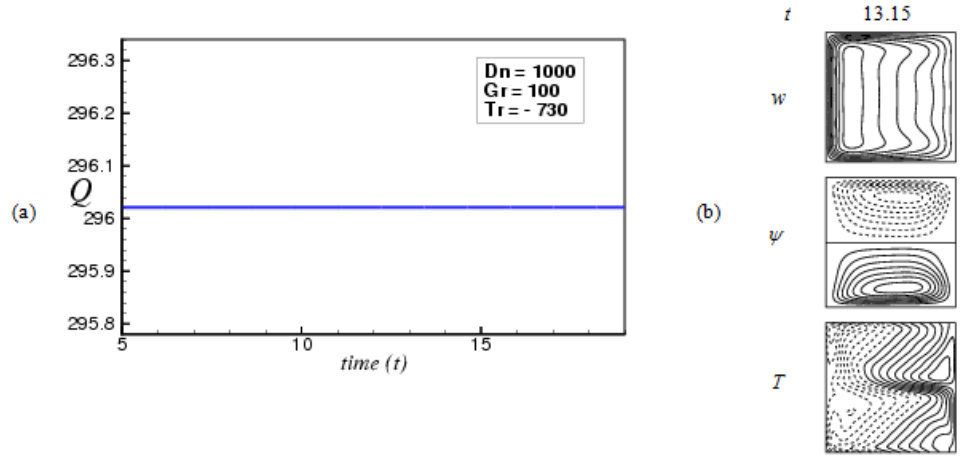

Fig. 16 (a) Time dependent behavior, (b) Contours of axial velocity (topmost), stream function (central) and isotherm (lowermost) for $Tr = -730$.

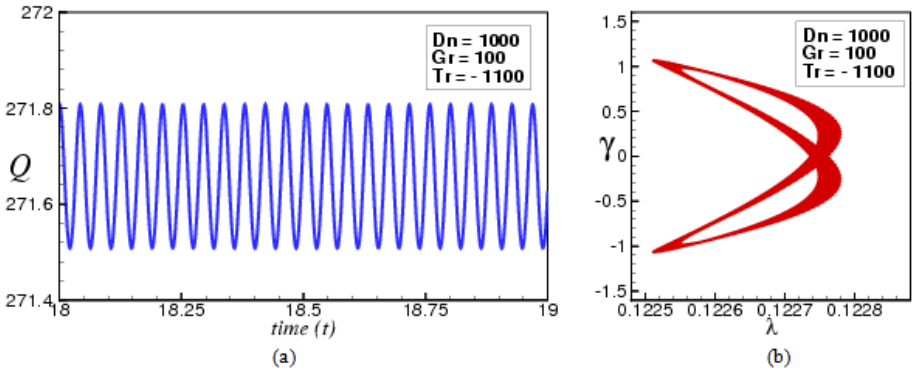

Fig. 17 (a) Time-dependent behavior and (b) Phase space for $Tr = -1100$.

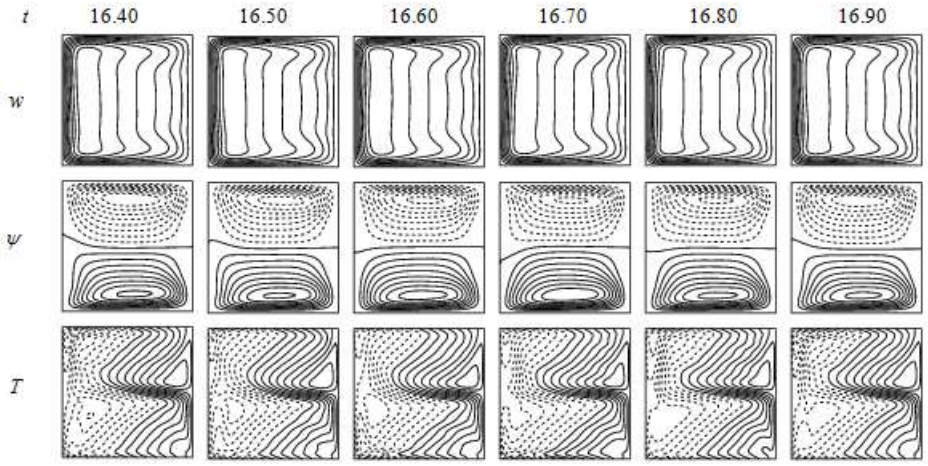

Fig. 18 Contours of axial velocity (topmost), stream function (central) and isotherm (lowermost) for $Tr = -1100$.

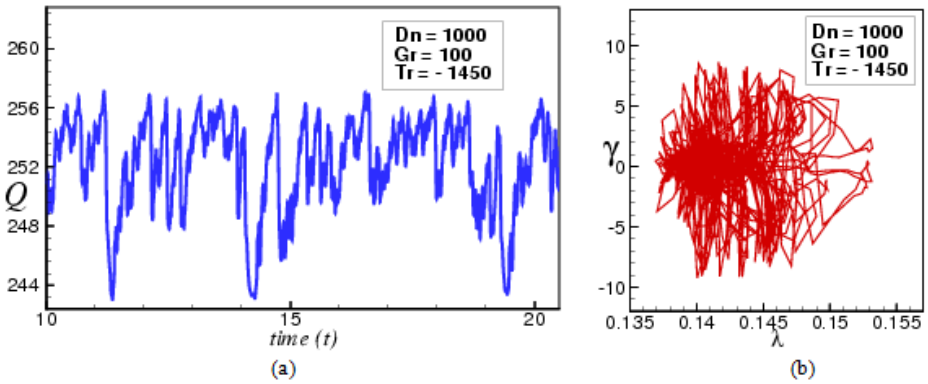

Fig. 19 (a) Time-dependent behavior and (b) Phase space for $Tr = -1450$.

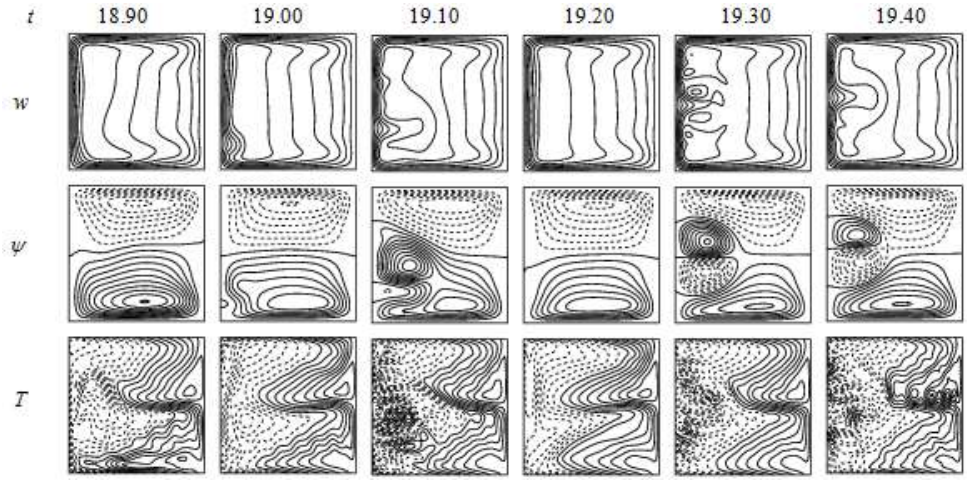

Fig. 20 Contours of axial velocity (topmost), stream function (central) and isotherm (lowermost) for $Tr = -1450$.

Now, we manifest time evolution calculation of the unsteady solution for $Tr = -730$, and it is found that the unsteady solution gives steady-state solution as shown in Figure 16(a). Axial flow, secondary flow and temperature profiles are explored in Figure 16(b) for $Tr = -730$.If the coriolis force is raised more in the negative direction, the steady-state solution switches to the periodic oscillation. Time evolution results for $Tr = -1100$ is displayed in Figure 17(a). To be clear more about the regular oscillation, phase spaces is enumerated as drawn in Figure 17(b). Phase space deliberates that the path lines meet at the starting point after completing an orbit. Two types of flow patterns axial and secondary flows, and the temperature profiles are shown in Figure 18. Then, we further explore unsteady characteristics for $Tr = -1450$. It is demonstrated that the unsteady solution delivers chaotic oscillation as shown in Figure 19(a). To have a clear insight into the flow, phase space is also calculated as depicted in Figure 19(b). Phase space narrates that the path of the stream flow is moved willingly in the $\lambda - \gamma$ plane, and the line spectrums oscillate continuously. Axial flow, secondary flow and temperature profiles are shown in Figure 20. As seen in Figure 20, 2- to 4-vortex solutions are found at $Tr = -1450$ where the dotted lines are seen in the upper wall of the duct and the additional vortices are situated in the inner wall of the duct. At $t = 19.10$ for $Tr = -1450$, axial flow regions are created at the top, so the secondary vortices are consisted at below. When the 4-vortex solutions are found the axial flows are divided into two high-velocity regions and the fluid are mixed up more than that of the two-vortex solution which is also seen by the temperature profiles. So the unsteady solutions do not demonstrate only the time-dependent solutions but also disclose a connection between the liner stability, axial flows, secondary flows and the heat transfer.

4.2 Bar Diagram of Vortex Structure

To observe the vortex-structure of secondary flows for unsteady solutions at a glance, we draw a bar diagram to show the vortex-structure in the *Taylor number vs. vortex* $(Tr-\theta)$ plane. Figure 21 shows vortex structure of secondary flows for unsteady solutions at $\delta = 0.015$. As seen in Figure 21, 2- to 4-vortex solutions are produced at the same value of *Tr* for both positive and negative rotation. These vortices are generated because of different types of forces including centrifugal, Coriolis and buoyancy forces. It is also noticed that increasing the number of vortices play an important role in fluid mixing as well as the enhancement of heat transfer in the flow.

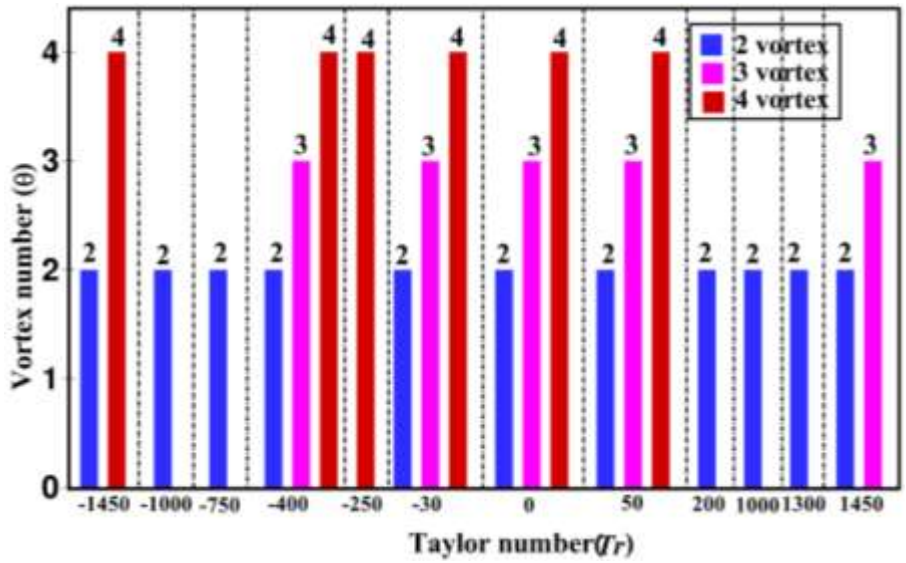

Fig. 21 Vortex structure of secondary flows for unsteady solutions at $\delta = 0.015$.

4.3 Heat Transfer

Heat transfer through the duct for both positive and negative rotation is calculated as shown in Figures 22(a) & 22(b), respectively. In the figures, the solid lines at the cooling and heating sidewalls are obtained from the steady solution branches that cover throughout the whole range of *Tr*. The symbols are found from the time average of unsteady solution for fixed *Tr*. It is demonstrated from the figures that heat is transferred more at negative rotation than that at the positive rotation for both cooling and heating walls. This is happened due to the rotation of the duct. Moreover, because of the advection in the duct, time-average of the transient flow at the cooling sidewall passes less heat than that at the cooling wall. On the other hand, there is a connection between the unsteady flow behavior and heat transfer. The heat at the regular and irregular oscillation for both cooling and heating wall is more than the steady-state solution. This is occurred because of fluid fixing. More precisely, the flows are vibrated more at the periodic, multi-periodic and chaotic oscillation than the steady-state solution. As a result, the fluid particles collide with each other and enhance heat transfer.

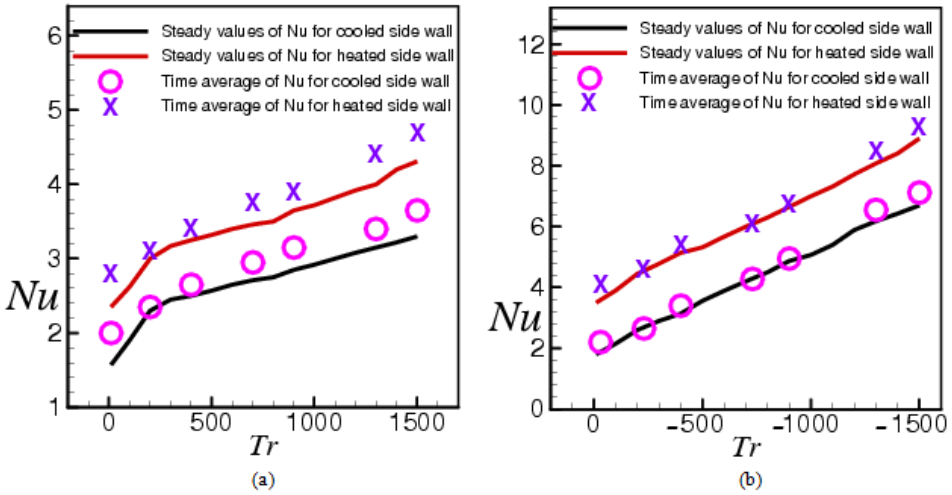

Fig. 22 Nusselt number variation for various *Tr*. (a) positive rotation, (b) negative rotation.

4.4 Validation of the Study

Here, numerical results are compared with the experimental outcomes to validate the current study. There are numerous authors who have disclosed the experimental outcomes on the curved square duct flow. Yamamoto et al. [43] investigated experimentally the rotating curved square duct flow. They adopted the visualization technique to explore the experimental outcome with a constant curvature $\delta = 0.3$. Yamamoto et al. [43] used a water flow tank where the dye was injected continuously and this dye was adjusted by the alcohol to be the same as the weight of water. At first, they fixed the rotation of the duct in the positive direction at $Tr = 150$ and took photographs at an angle 180° inlet for several values of Dn. The same work was then conducted for negative rotation at $Tr = -150$. In the present study, we fix our parameters according to that Yamamoto et al [43] experimented. Then we obtain the numerical outcome of the secondary flow for several values of *Dn* as shown in Figure 23 and it is observed that there is a good matching between the numerical and experimental investigation.

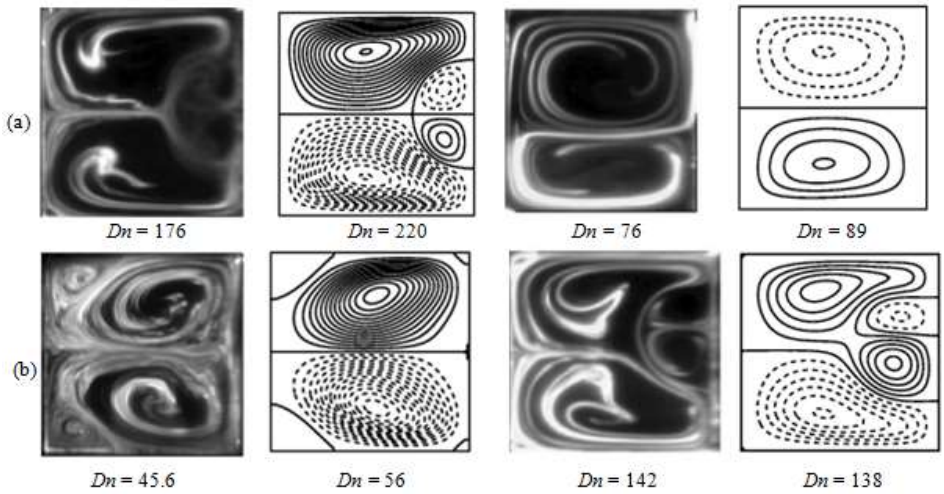

Fig. 23 Experimental (left, Yamamoto et al. [43]) vs. numerical (right, authors) results for rotating curved square duct flow; (a) *Tr* = 150, (b) *Tr* = - 150.

5. DISCUSSIONS

The study of flow characteristics in a curved duct is a fundamental interest of engineering community because it has a wide range of real-life applications including heat exchangers, chemical mixing, power industry, rotating electrical machinery etc. not to mention application in other areas such as blood flow in human vein and arteries. The researchers are therefore interested to investigate different types of phenomena by changing the governing equations. Here, we discuss contributions and limitations of some papers published in literature and tried to explain what is new in the ongoing exploration. Yang et al. [44] used CFD based Fluent software and user-defined function to expose flow vibration and time-dependent flow configuration through a circular cylinder. Khanafer et al. [45] conducted Nk5000 code to explore the effect in streamlines and isotherms with changing parameters and showed that the rotational speed expressively enhances overall heat throughout the fluid than other parameters such as Richardson number and the Reynolds number. Bibin et al. [46] used vector plot to represent the axial velocity and showed temperature contour at several axial locations. Umavathi and Beg [47] applied finite difference method to demonstrate viscous and buoyancy effects in the secondary and isotherm contour for non-isothermal flow through a vertical duct. Nobari et al. [48] analyzed pattern variation of axial and secondary flow in annular duct at different inlets. They also calculated heat transfer in the duct but they did not visualize the isotherm variation in their exploration. Riyi et al. [49] elucidated heat transport and temperature profiles in the inner and outer inlet of the curved annular duct experimentally for a wide range of Reynolds number. Mansour et al. [50] discussed the fluid mixing in three different tubes for several Dean numbers over a wide range of the Reynolds numbers but flow velocity as well as contours of fluid mixing were absent in their study. Tanweer et al. [51] performed unsteady behavior with respect to drag and lift coefficient and observed

heat transfer when the cylinder is near the moving wall. Though their study discussed heat transfer in three-dimensional coordinate system, the investigation is limited for low Reynolds number. Hasan et al. [52-54] adopted spectral technique to explore time-dependent behavior of fluid flow through rotating and non-rotating curved ducts with detail explanation on curvature and heating-induced buoyancy effects. To the best of the authors' knowledge, however, there is no known study that describes hydrothermal behavior of transient fluid flow and energy distribution with forced convection through a rotating curved square duct with rotational effects, which is successfully accomplished in the ongoing paper. Besides, a relationship between the axial flow, secondary flow and isotherms is established, and it is revealed that heat transfer is certainly influenced by the rotation of the duct and overall heat transfer is significantly enhanced as the rotation is increased, which is absent in literature till now. The present study may improve the knowledge in heat generation and transfer that constitute a new epoch in fluids engineering to produce energy-related machinery.

6. CONCLUSION

A spectral-based computational technique is implemented to study time-dependent flow and heat transfer through a rotating curved square duct with small curvature. The lower wall of the duct is heated while cooling from the upper, the inner and outer walls being thermally insulated to present heat loss. The system is rotated about the vertical axis in the positive and negative direction for the Taylor number, $-1500 \le Tr \le 1500$. The numerical results are validated with the available experimental data and a good matching is noticed. The following conclusions have been drawn from the present study;

- Time-development flow as well as phase-space of the time progression results shows that the transient flow endures in the consequence "*multi-periodic* $\rightarrow$ *steady state* $\rightarrow$ *periodic* $\rightarrow$ *multi-periodic* $\rightarrow$ *chaotic*", if Tr is increased in the positive direction; for negative rotation, however, the flow experiences the evolution "*multi-periodic* $\rightarrow$ *steady state* $\rightarrow$ *multi-periodic* $\rightarrow$ *steady state* $\rightarrow$ *periodic* $\rightarrow$ *chaotic*".
- Flow instability at negative rotation shows more transiency than that at positive rotation, and it is found that the regular and irregular oscillation at high rotation becomes stronger than that at small rotation.
- 2- to 6-vortex solutions are generated at the periodic, multi-periodic and chaotic flows, and the number of secondary vortices is significantly higher for the chaotic solutions while few for the steady-state solution.
- A strong bond between the axial and the secondary flow has been established for regular and irregular oscillation which agrees well with temperature distribution. The study shows that heat transfer occurs prominently if the rotation is increased either in the positive or in the negative direction.
- A strong dominance among heating-induced buoyancy force and centrifugal-Coriolis instability is observed that augments flow interaction and enriches heat transfer in the flow. The study reveals that chaotic solutions boost heat transfer more effectively than the steady-state or other physically realizable solutions due to formation of significant number of Dean vortices at the outer concave wall.

REFERENCES

1. Mondal, R.N., Kaga, Y., Hyakutake, T., Yanase, S., 2006, *Effects of curvature and convective heat transfer in curved square duct flows*, Trans ASME, Journal of Fluids Engineering, 128(9), pp. 1013-1022. https://doi.org/10.1115/1.2236131
2. Mondal, R.N., Kaga, Y., Hyakutake, T., Yanase, S., 2007, *Bifurcation diagram for two-dimensional steady flow and unsteady solutions in a curved square duct*, Fluid Dynamics Research, 39, pp. 413-446. https://doi.org/10.1016/j.fluiddyn.2006.10.001
3. Yanase, S., Mondal, R.N., Kaga, Y., 2005, *Numerical Study of Non-Isothermal Flow with Convective Heat Transfer in a Curved Rectangular Duct*, International Journal of Thermal Science, 44(11), pp. 1047-1060. https://doi.org/10.1016/j.ijthermalsci.2005.03.013
4. Rumsey, C.L., Gatski, T.B., Morrison, J.H., 2010, *Turbulence Model Predictions of Strongly Curved Flow in a U-Duct*, AIAA Journal, 38(8), pp. 1394-1402. https://doi.org/10.2514/2.1115
5. Chandratilleke, T.T., Nadim, N., Narayanaswamy, R., 2013, *Analysis of Secondary Flow Instability and Forced Convection in Fluid Flow through Rectangular and Elliptical Curved Ducts*, Heat Transfer Engineering, 34(14), pp. 1237-1248. https://doi.org/10.1080/01457632.2013.777249
6. Ahmadloo, E., Sobhanifar, N., Hosseini, F.S., 2014, *Computational Fluid Dynamics Study on Water Flow in a Hollow Helical Pipe*, Open Journal of Fluid Dynamics, 4(2), pp. 133-139. https://doi.org/10.4236/ojfd.2014.42012
7. Liu, F., Wang, L., 2009, *Analysis on multiplicity and stability of convective heat transfer in tightly curved rectangular ducts*, International Journal of Heat and Mass Transfer, 52(25-26), pp. 5849–5866. https://doi.org/10.1016/j.ijheatmasstransfer.2009.07.019
8. Yanase, S., Kaga, Y., Daikai, R., 2002, *Laminar flow through a curved rectangular duct over a wide range of aspect ratio*, Fluid Dynamics Research, 31(3), pp. 151-83. https://doi.org/10.1016/S0169-5983(02)00103-X
9. Yanase, S., Watanabe, T., Hyakutake, T., 2008, *Traveling-wave solutions of the flow in a curved-square duct*, Physics of Fluids, 20(12), 124101. https://doi.org/10.1063/1.3029703
10. Nazeer, G.., Islam, S., Shigri, S.H., Saeed, S., 2019, *Numerical investigation of different flow regimes for multiple staggered rows*, AIP Advances, 9(3), 035247. https://doi.org/10.1063/1.5091668
11. Zhou, B., Wang, X., Guo, W., Gho, W.M., Tan, S.K., 2015, *Control of flow past a dimpled circular cylinder*, Experimental Thermal and Fluid Science, 69, pp. 19–26. http://dx.doi.org/10.1016/j.expthermflusci.2015.07.020
12. Zhang, J., Chen, H., Zhou, B., Wang, X., 2019, *Flow around an array of four equispaced square cylinders*, Applied Ocean Research, 89, pp. 237-250. https://doi.org/10.1016/j.apor.2019.05.019
13. Hashemi, A., Fischer, P.F., Loth, F., 2018, *Direct numerical simulation of transitional flow in a finite length curved pipe*, Journal of Turbulence, 19(8), pp. 664-682. https://doi.org/10.1080/14685248.2018.1497293
14. Zhang, W., Wei, Y., Dou, H.S., Zhu, Z., 2018, *Transient behaviors of mixed convection in a square enclosure with an inner impulsively rotating circular cylinder*, International Communications in Heat and Mass Transfer, 98, pp. 143-154. https://doi.org/10.1016/j.icheatmasstransfer.2018.08.016
15. Wang, L., Yang, T., 2005, *Periodic oscillation in curved duct flows*, Physica D, 200, pp. 296–302. https://doi.org/10.1016/j.physd.2004.11.003
16. Arpino, F., Cortellessa, G,., Mauro, A., 2015, *Transient Thermal Analysis of Natural Convection in Porous and Partially Porous Cavities*, Numerical Heat Transfer, Part A: Applications, 67(6), pp. 605-631. https://doi.org/10.1080/10407782.2014.949133
17. Mondal, R.N., Islam, M.S., Uddin, K., Hossain, M.A., 2013, *Effects of aspect ratio on unsteady solutions through curved duct flow*, Applied Mathematics and Mechanics, 34(9), pp. 1107-1122. https://doi.org/10.1007/s10483-013-1731-8
18. Ray, S.C., Hasan, M.S., Mondal, R.N., 2020, *On the Onset of Hydrodynamic Instability with Convective Heat Transfer Through a Rotating Curved Rectangular Duct*, Mathematical Modelling of Engineering Problems, 7(1), pp. 31-44. https://doi.org/10.18280/mmep.070105
19. Hasan, M.S., Islam, M.M., Ray, S.C., Mondal, R.N., 2019, *Bifurcation structure and unsteady solutions through a curved square duct with bottom wall heating and cooling from the ceiling*, AIP Conference Proceedings, 2121, 050003. https://doi.org/10.1063/1.5115890
20. Hasan, M.S., Mondal, R.N., Lorenzini, G., 2019, *Numerical Prediction of Non-isothermal Flow with Convective Heat Transfer through a Rotating Curved Square Channel with Bottom Wall Heating and*

Cooling from the Ceiling, International Journal of Heat and Technology, 37(3), pp. 710-726. https://doi.org/10.18280/ijht.370307

21. Islam, M.Z., Mondal, R.N., Rashidi, M.M., 2017, *Dean-Taylor Flow with Convective Heat Transfer through a Coiled Duct*, Computers and Fluids, 149, pp. 141-155. https://doi.org/10.1016/j.compfluid.2017.03.001
22. Kurtulmus, N., Zontul, H., Sahin, B., 2020, *Heat transfer and flow characteristics in a sinusoidally curved converging-diverging channel*, International Journal of Thermal Sciences, 148, 106163. https://doi.org/10.1016/j.ijthermalsci.2019.106163
23. Zheng, Y., Jiang, P.X., Luo, F., Xu, R.N., 2019, *Instability during transition to turbulence of supercritical pressure CO2 in a vertical heated serpentine tube*, International Journal of Thermal Sciences, 145, 105976. https://doi.org/10.1016/j.ijthermalsci.2019.105976
24. Dean, W.R., 1927, *Note on the motion of fluid in a curved pipe*, Philos Mag., 4, pp. 208-23. https://doi.org/10.1080/14786440708564324
25. Ozaki, K., Maekawa, H., 2004, *Curvature Effects in the Curved Duct for the Compressible Viscous Flow*, 24th International Congress of the Aeronautical Sciences, pp. 1787-1792. https://doi.org/10.1115/FEDSM2003-45634
26. Chandratilleke, T.T., Nadim, N., Narayanaswamy, R., 2012, *Vortex structure-based analysis of laminar flow behaviour and thermal characteristics in curved ducts*, International Journal of Thermal Sciences, 59, pp. 75-86. https://doi.org/10.1016/j.ijthermalsci.2012.04.014
27. Alam, M.M., Ota, M., Ferdows, M., Islam, M.N., Wahiduzzaman, M., Yamamoto, K., 2007, *Flow through a rotating helical pipe with a wide range of the Dean number*, Arch. Mech., 59(6), pp. 501–517.
28. Bayat, P., Rezai, P., 2017, *Semi-Empirical Estimation of Dean Flow Velocity in Curved Microchannels*, Scientific Reports, 7, 13655. https://doi.org/10.1038/s41598-017-13090-z
29. Li, Y., Wang, X., Yuan, S., Tan, S.K., 2016, *Flow development in curved rectangular ducts with continuously varying curvature*, Experimental Thermal and Fluid Science, 75, 1–15. https://doi.org/10.1016/j.expthermflusci.2016.01.012
30. Watanabe, T., Yanase, S., 2013, *Bifurcation Study of Three-Dimensional Solutions of the Curved Square-Duct Flow*, Journal of the Physical Society of Japan, 82, 074402, pp. 1-9. https://doi.org/10.7566/JPSJ.82.074402
31. Nowruzi, H., Ghassemi, H., Nourazar, S.S., 2020, *Study of the effects of aspect ratio on hydrodynamic stability in curved rectangular ducts using energy gradient method*, Engineering Science and Technology, 23(2), 334-344. https://doi.org/10.1016/j.jestch.2019.05.004
32. Norouzi, M., Biglari, N., 2013, *An analytical solution for Dean flow in curved ducts with rectangular cross section*, Physics of Fluids, 25, 053602. https://doi.org/10.1063/1.4803556
33. Razavi, S.E., Soltanipour, H., Choupania, P., 2015, *Second Law Analysis of Laminar Forced Convection in a Rotating Curved Duct*, Thermal Science, 19(1), pp. 95-107. https://doi.org/10.2298/tsci120606034r
34. Hasan, M.S., Mondal, R.N., Lorenzini, G.., 2019, *Centrifugal Instability with Convective Heat Transfer Through a Tightly Coiled Square Duct*, Mathematical Modelling of Engineering Problems, 6(3), pp. 397-408. https://doi.org/10.18280/mmep.060311
35. Hasan, M.S., Mondal, R.N., Kouchi, T., Yanase, S., 2019, *Hydrodynamic instability with convective heat transfer through a curved channel with strong rotational speed*, AIP Conference Proceedings, 2121, 030006. https://doi.org/10.1063/1.5115851
36. Sasmito, A.P., Kurnia, J.C., Mujumdar, A.S., 2011, *Numerical evaluation of laminar heat transfer enhancement in nanofluid flow in coiled square tubes*, Nanoscale Research Letters, 6(376). https://doi.org/10.1186/1556-276X-6-376
37. AL-Juhaishi, L.F.M., Ali, M.F.M., Mohammad, H.H., Ajeel, R.K., 2020, *Numerical thermal-hydraulic performance investigations in turbulent curved channel flow with horseshoe baffles*, Heat transfer, 49(6), pp. 3816-3836. https://doi.org/10.1002/htj.21810
38. Zhang, L.Y., Lu, Z., Wei, L.C., Yang, X., Yu, X.L., Meng, X.Z., Jin, L.W., 2019, *Numerical investigation of flow characteristics and heat transfer performance in curve channel with periodical wave structure*, International Journal of Heat and Mass Transfer, 140, pp. 426–439. https://doi.org/10.1016/j.ijheatmasstransfer.2019.05.117
39. Zhang, C., Niu, Y., Xu, J., 2020, *An anisotropic turbulence model for predicting heat transfer in a rotating channel*, International Journal of Thermal Sciences, 148, 106119. https://doi.org/10.1016/j.ijthermalsci.2019.106119

40. Schindler, A., Younis, B.A., Weigand, B., 2019, *Large-Eddy Simulations of turbulent flow through a heated square duct*, International Journal of Thermal Sciences, 135, pp. 302-318. https://doi.org/10.1016/j.ijthermalsci.2018.09.018
41. Gottlieb, D., Orazag, S.A., 1977, *Numerical Analysis of Spectral Methods*, Society of Industrial and Applied Mathematics, Philadelphia, USA. https://doi.org/10.1137/1.9781611970425
42. Mondal,, R.N., 2006, *Isothermal and Non-isothermal Flows through Curved ducts with Square and Rectangular Cross Sections*, Ph.D. Thesis, Department of Mechanical and Systems Engineering, Okayama University, Japan.
43. Yamamato, K., Xiaoyum, W., Kazou, N., Yasutuka, H., 2006, *Visualization of Taylor-Dean flow in a curved duct of square cross section*, Fluid Dynamics Research, 38, pp. 1-18. https://doi.org/10.1016/j.fluiddyn.2005.09.002
44. Yang, Z., Ding, L., Zhang, L., Yang, L., He, H., 2020, *Two degrees of freedom flow-induced vibration and heat transfer of an isothermal cylinder*, International Journal of Heat and Mass Transfer, 154, 119766. https://doi.org/10.1016/j.ijheatmasstransfer.2020.119766
45. Khanafer, K., Aithal, S.M., Vafai, K., 2019, *Mixed convection heat transfer in a differentially heated cavity with two rotating cylinders*, International Journal of Thermal Sciences, 135, pp. 117-132. https://doi.org/10.1016/j.ijthermalsci.2018.07.020
46. Bibin, K.S., Jayakumar, J.S., 2020, *Thermal hydraulic characteristics of square ducts having porous material inserts near the duct wall or along the duct centre*, International Journal of Heat and Mass Transfer, 148, 119079. https://doi.org/10.1016/j.ijheatmasstransfer.2019.119079
47. Umavathi, J.C., Bég, O.A., 2020, *Effects of thermo-physical properties on heat transfer at the interface of two immisicible fluids in a vertical duct: Numerical study*, International Journal of Heat and Mass Transfer, 154, 119613. https://doi.org/10.1016/j.ijheatmasstransfer.2020.119613
48. Nobari, M.R.H., Ahrabi, B.R., Akbari, G., 2009, *A numerical analysis of developing flow and heat transfer in a curved annular pipe*, International Journal of Thermal Sciences, 48: 1542–1551. https://doi.org/10.1016/j.ijthermalsci.2008.12.004
49. Riyi, L., Xiaoqian, W., Weidong, X., Xinfeng, J., Zhiying, J., 2019, *Experimental and numerical study on forced convection heat transport in eccentric annular channels*, International Journal of Thermal Sciences, 136: 60-69. https://doi.org/10.1016/j.ijthermalsci.2018.10.003
50. Mansour, M., Thévenin, D., Zähringer, K., 2020, *Numerical study of flow mixing and heat transfer in helical pipes, coiled flow inverters and a novel coiled configuration*, Chemical Engineering Science, 221, 115690. https://doi.org/10.1016/j.ces.2020.115690
51. Tanweer, S., Dewan, A., Sanghi, S., 2020, *Influence of three-dimensional wake transition on heat transfer from a square cylinder near a moving wall*, International Journal of Heat and Mass Transfer, 148, 118986. https://doi.org/10.1016/j.ijheatmasstransfer.2019.118986
52. Hasan, M.S., Mondal, R.N., Lorenzini, G., 2020, *Physics of bifurcation of the flow and heat transfer through a curved duct with natural and forced convection*, Chinese Journal of Physics, 67, pp. 428-457. https://doi.org/10.1016/j.cjph.2020.07.004
53. Hasan, M.S., Islam, M.S., Badsha, M.F., Mondal, R.N., Lorenzini, G., 2020, *Numerical Investigation on the Transition of Fluid Flow Characteristics Through a Rotating Curved Duct*, International Journal of Applied Mechanics and Engineering, 25(3), pp. 45-63. https://doi.org/10.2478/ijame-2020-0034
54. Hasan, M.S., Mondal, R.N., Lorenzini, G., 2020, *Coriolis force effect in steady and unsteady flow characteristics with convective heat transfer through a curved square duct*, International Journal of Mechanical Engineering, 5(1), pp. 1-39.